Heliyon 7 (2021) e08197

Contents lists available at ScienceDirect

Heliyon

journal homepage: www.cell.com/heliyon

Research article

Antimicrobial and antihemolytic properties of a CNF/AgNP-chitosan film: A potential wound dressing material

Poppy Anjelisa Zaitun Hasibuan [a,*], Yuandani [a], Masitta Tanjung [b], Saharman Gea [c,d], Khatarina Meldawati Pasaribu [c,d], Mahyuni Harahap [c,d], Yurika Almanda Perangin-Angin [c,d], Andre Prayoga [a], Junius Gian Ginting [a]

[a] Department of Pharmacology, Faculty of Pharmacy, Universitas Sumatera Utara, Jl. Tridharma No.5, Medan, 22919, Indonesia
[b] Department of Biology, Faculty of Mathematics and Natural Science, Universitas Sumatera Utara, Jl. Bioteknologi No.1, Medan, 20155, Indonesia
[c] Cellulosic and Functional Materials Research Centre, Universitas Sumatera Utara, Jl. Bioteknologi No.1, Medan, 20155, Indonesia
[d] Department of Chemistry, Faculty of Mathematics and Natural Science, Universitas Sumatera Utara, Jl. Bioteknologi No.1, Medan, 20155, Indonesia

GRAPHICAL ABSTRACT

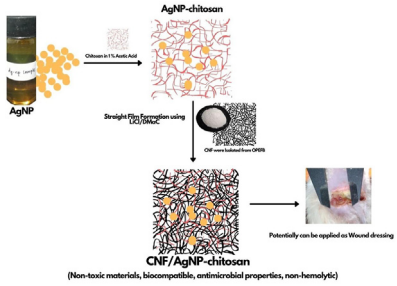

ARTICLE INFO

Keywords:
Cellulose nanofibers
Chitosan
Silver nanoparticle
Film
Wound dressing

ABSTRACT

Cellulose nanofibers (CNFs), chitosan, and silver nanoparticles (AgNPs) are widely used to enhance the active functions and antibacterial properties of wound dressings. This study was conducted to prepare CNF/AgNP-chitosan using a straight incorporation method and to assess its antimicrobial activity. CNFs were isolated from oil palm empty fruit bunches (OPEFBs) using the pulping method and acid hydrolysis. AgNPs were synthesized using a green synthesis method. The wound dressing was produced by mixing a 10% CNF solution in LiCl/DMAc and AgNP-chitosan in a glass plate with various ratios of CNF/AgNP-chitosan, i.e., 100:0, 80:20, 60:40, and 50:50. UV-visible and TEM analyses were conducted to confirm the formation of AgNPs and CNFs at the nanoscale. The results showed particles with an absorption wavelength of 435 nm and spherical shapes. Based on the calculation using ImageJ software, the diameters of CNFs were approximately 50 nm, and the lengths were several micrometers. FTIR was used to analyze the chemical bonding of AgNP-chitosan and the incorporated AgNP-chitosan in CNFs. Based on the XRD analysis, the presence of AgNPs did not affect the crystallinity of the CNFs. SEM images showed that the addition of AgNPs resulted in the stretching of CNF pores on the pads. Thermal degradation of the film increased with the addition of AgNP-chitosan by up to 40%. Antimicrobial tests and hemocompatibility tests showed that the formed CNF/AgNP-chitosan film successfully inhibited bacterial growth and was classified as a nonhemolytic material; thus, its potential as a wound dressing should be further studied.

* Corresponding author.
E-mail address: poppyanjelisa@usu.ac.id (P.A. Zaitun Hasibuan).

https://doi.org/10.1016/j.heliyon.2021.e08197
Received 8 June 2021; Received in revised form 3 September 2021; Accepted 14 October 2021

1. Introduction

Wound dressing is an effective alternative for patients who require wound healing treatment because it has been shown to speed up the healing process [1]. Research on wound dressings using films, hydrogels and nanofibers synthesized with the electrospinning method has recently been conducted and has been shown to be successful and to play an important role in the wound healing process [2]. Various materials that are abundantly found in nature and easily processed, i.e., cellulose, chitosan, collagen, alginate, AgNPs, and PVA, have become popular materials for wound dressings since they also have high biocompatibility [3, 4, 5, 6, 7, 8].

In general, a good wound dressing must meet a number of conditions, such as preventing the growth of pathogenic bacteria and absorbing the exudate of the wound while still maintaining the moisture content of the wound, supporting the process of tissue regeneration and accelerating the process of wound healing [9, 10, 11]. Nanomaterials, such as AgNPs, have recently sparked interest because the synthesis process is capable of being carried out and conditioned in a variety of ways, depending on the needs and subsequent use [5, 8, 12, 13]. Several studies have also shown that AgNPs have the potential to be used in the wound healing process, as they are reported to have good antibacterial properties against both gram-negative and gram-positive pathogens and to effectively inhibit biofilm growth by *Enterobacter cloacae*, *Streptococcus thermophiles*, and *Propionibacterium acnes,* bacteria that are commonly found in wounds [1, 14, 15].

Previous research has also shown that AgNP incorporation in membrane AgNP–BCs effectively accelerates the growth of epidermal tissue and skin dermis in wound areas twice as fast as in wounds without treatment [16]. An explanation for this finding is that AgNPs induce cell proliferation in the wound healing process. In addition, based on the results of quantitative PCR, proteomic and immunohistochemistry studies [17], AgNPs are also reported to minimize inflammation in wounds and accelerate re-epithelization and regulation of fibrogenic cytokines, accelerating the wound healing process and facilitating the resulting wound closure [18].

Although AgNPs have many benefits in accelerating wound healing, supporting components, such as the matrix, in the impregnation process of AgNPs must also be considered. Previous studies using AgNPs as wound dressings showed that AgNPs are often prepared as nanocomposites, immobilized membranes, incorporated mats, films and hydrogels [18].

CNFs are promising materials that are also widely used as biomaterials due to their biocompatible properties. Moreover, CNFs were also considered a matrix in this study since their fibers meet wound dressing requirements [19]. CNFs potentially represent a good barrier to protect wounds from contaminants, cover wounds, absorb wound exudates and a good template for impregnated AgNPs. CNF is also considered since it would make dressing replacement and removal more convenient and less painful, thus preventing the risk of secondary trauma and wound infections in the healing process [20, 21].

However, a number of studies also indicate the vulnerability of AgNPs, as they appear to be unstable [2, 22, 23, 24]. Chitosan was suggested as an additional material to increase the stability of AgNPs. Chitosan forms thin filaments on the surface of AgNPs and increases their stability [25]. Moreover, the addition of chitosan as a material for wound dressing applications is also beneficial, as chitosan is nontoxic, biodegradable, biocompatible and has good antibacterial activity [26]. Thus, in the present study, chitosan not only serves as an AgNP stabilizer but also plays an active role in the wound healing process.

In this study, AgNPs were coated with chitosan to increase their stability. After the AgNPs that had been coated with chitosan, they were integrated into the CNF film. The matrix of the CNF/AgNP-chitosan film was studied as an antimicrobial agent, and its hemocompatibility was assessed to potentially be used as a wound dressing. This study received attention since no previous studies have identified either the straight film formation of CNF/AgNP-chitosan itself or its possibility to be applied as a wound dressing.

2. Materials and methods

2.1. Materials

Cellulose nanofibers (CNFs) from oil palm empty fruit bunches (OPEFBs) were isolated using the pulping method followed by acid hydrolysis [27]. The materials used in this study were $DMaC_{(aq)}$, $AgNO_{3(s)}$, $starch_{(s)}$, acetic $acid_{(l)}$, $HNO_{3(aq)}$, $NaNO_{2(s)}$, $Na_2SO_{3(s)}$, $NaOCl_{(aq)}$, $H_2O_{2(aq)}$ 30%, and $LiCl_{(s)}$ purchased from Merck (Darmstadt, Germany). The chitosan used in this experiment was purchased from Acros Organics, China.

2.2. The isolation of CNFs

Oil palm empty fruit bunches (OPEFB) were dried and cut into small pieces approximately 1 cm in length. Then, 75 g of dried OPEFB were physically treated using the steam explosion method described in our previous study to isolate CNFs from lignin, hemicellulose and other chemicals contained in bunches [27]. CNFs produced using this approach were shown to form thin nanoscale fibers. The fibers were then washed with deionized water until the pH was approximately 7. The final product was dried in a vacuum oven at 50 °C for 5 h and stored in a desiccator until further use.

2.3. The preparation of AgNPs

The AgNP synthesis process used in this study was adapted from Handoko et al., 2019 [23]. Silver nanoparticles (AgNPs) were prepared by mixing $AgNO_3$ and glucose at a 1:1 composition ratio. Then, 80 mL of the mixture were transferred to a glass beaker, and 20 mL of starch 1% were added. Next, the mixture was constantly stirred in close and dark conditions at 90 °C for 4 h. Afterward, the sample was cooled at room temperature and centrifuged at 5000 rpm for 10 min. The product was collected for further characterization. The AgNP solution obtained in this study was brownish yellow.

2.4. The preparation of AgNP-chitosan

First, 2 g of chitosan were dissolved in 1% acetic acid through constant stirring at room temperature for 1 h. When the chitosan had completely dissolved, 10 mL of AgNPs were added dropwise to the chitosan solution.

2.5. The preparation of CNF/AgNP-chitosan film

First, 8% LiCl was dissolved in DMAc at room temperature for 3 h. After LiCl was gently dissolved in DMAc, CNFs were added and stirred at room temperature for 3 h. After CNFs were completely dissolved in the LiCl/DMAc solution, AgNP-chitosan was added. CNF/AgNP-chitosan was produced at ratios of 100:0, 80:20, 60:40, and 50:50 v/v. The solution was then poured into a film molding plate. The film was then dried at 50 °C for 5 h in a vacuum oven. The produced film was then analyzed for toxicity by immersion in water, and the water was changed. The pH was tested every day to ensure that it was safe for use in medical applications.

2.6. Characterizations

2.6.1. Scanning electron microscopy (SEM)

The morphology of the formed samples in this study was then observed using SEM EDX EVO MA Zeiss Bruker in Mabes Polri, Jakarta Indonesia. The sample was prepared by coating it with gold, and the analysis was conducted using a 20 kV voltage system.

2.6.2. Fourier transform-infrared (FTIR) spectroscopy

Functional groups of formed samples were recorded using Platinum-ATR (Bruker, Alpha) at wavelengths ranging from 400-4000 cm-1 in 100 scans. The curve was then plotted using Orign Pro 2016 Software.

2.6.3. X-ray diffraction (XRD)

The 2θ angles of the samples were analyzed at 0–70° using a Shimadzu XRD-6100 diffractometer with a scanning rate of 0.02 s^{-1} at 35 kV and 25 mA to study the crystallinity properties. The analysis was performed at Central Laboratory UNIMED, Medan, Indonesia.

2.6.4. Thermogravimetric analysis

The thermal properties of the formed samples were studied using a Setting EXTAR 7300 Series machine with temperatures ranging from 30-600 °C and a 10 °C/min heating rate under nitrogen gas conditions.

2.6.5. Transmission electron microscopy

The AgNPs were investigated using a LoJeol 1200 EX transmission electron microscope (TEM). The instrument was operated using an accelerating voltage of 80 kV.

2.6.6. UV-visible spectroscopy

The UV-visible spectra of the formed samples were recorded using a Shimadzu Scientific Instrument (UV 1800 series) ultraviolet/visible spectrophotometer. The samples were diluted and measured at wavelengths ranging from 200 to 800 nm.

2.7. Antimicrobial properties

All samples were subjected to a disc diffusion test with some gram-negative (*Pseudomonas aeruginosa*) and gram-positive (*Bacillus subtilis*) bacteria and fungi (*Candida albicans*) to investigate the antimicrobial properties of CNF/AgNP-chitosan.

2.7.1. Antibacterial activity

The antibacterial test used in this study was conducted by pouring the nutrient media into a Petri dish. The nutrient media were then swabbed with *P. aeruginosa* and *B. subtilis*, and each pad was cut into 6 mm paper discs and placed on the surface of the media. All samples were then incubated at 36–37 °C for 24 h. The resulting inhibition zone was measured using a caliper [28]. Gentamicin 0.1% was used as a positive control [29], and CNF/AgNP-chitosan (100:0) was used as a negative control.

2.7.2. Antifungal activity

The culture of *Candida albicans* in potato dextrose broth (PDB) medium was prepared as dilution of 10^0 to 10^{-7}. These dilutions were prepared to obtain the number of colonies in 1 mL before testing. In the diffusion test, the standard inoculation amount tested was 1–2 × 10^8 CFU/mL [30]. The dilution of *Candida albicans* was consistent with the test standards (100 μL) applied using a micropipette, poured into Sabouraud dextrose agar (SDA) media in a Petri dish and then flattened using a spreader. Then, the cells were incubated for 2 × 24 h at room temperature. Each pad was cut into a paper disc (6 mm) and then placed in SDA media in a Petri dish containing the *Candida albicans* fungal culture. Ketoconazole 2% was used as a positive control [31], and patch 100:0 was used as a negative control. Then, samples were incubated for 24 h at 37 °C. Furthermore, the inhibition zone was measured using calipers, and the diameter was calculated.

2.8. Hemocompatibility test

A hemocompatibility test was performed to measure the compatibility of the film while in direct contact with blood and to assess the potential of the film to be applied as a wound dressing. The anticoagulated horse blood was dissolved in 0.9% saline and centrifuged at 3000 rpm for 10 min. In addition, the sample was soaked in a saline solution for 2 h at 37 °C with agitation. All samples were then measured at a wavelength of 540 nm, including blood diluted in distilled water and normal saline, which were used as positive and negative controls in this study. Hemolysis was then calculated with Formula (1).

$$\text{Hemolysis } (\%) = (\text{Af-Ac(-)})/(\text{Ac(+)-Ac(-)}).\ 100 \quad (1)$$

where

A_f = Absorbance of the film.
$A_{c(-)}$ = Absorbance of the control (-)
$A_{c(+)}$ = Absorbance of the control (+).

3. Results

3.1. Morphological analysis

CNFs isolated from OPEFB with the steam explosion method successfully produced tiny fibers, as shown in Figure 1 (a). For further analyses, TEM micrographs were obtained for CNFs, as presented in Figure 1 (b). The micrograph strongly supported the hypothesis that the CNF extraction process using acid hydrolysis to form α-cellulose removed the amorphous part from the crystalline structure of the formed CNFs. Based on the calculation using ImageJ analysis, the diameters of CNFs were approximately 50 nm, and the lengths were several micrometers. A similar result was obtained in our previous study, in which CNFs were isolated from OPEFB using steam explosion [27, 32].

Figure 1 (c) shows the solution of AgNPs prepared in this study using green synthesis. Several studies also mentioned the color transformation of the colorless $AgNO_3$ solution to a brown solution containing AgNPs. The TEM images in Figure 1 (d) show that AgNPs were successfully prepared in this study. The formed AgNPs exhibited spherical shapes with a diameter distribution ranging from 10-50 nm, as displayed in Figure 1 (e). UV-visible spectroscopy, which was performed on the AgNP sample in this study, showed that the surface plasmon resonance (SPR) value of AgNPs was 435 nm (Figure 1 (f)). This result was consistent with a study reporting that the SPR value of AgNPs ranged from 410-450 nm and that the nanoparticles presented spherical shapes [23].

The morphology of the samples was further studied using scanning electron microscopy (SEM), as shown in Figure 2.

Figure 2 (a) shows the SEM image of pure CNF fibers. In the CNF image, every nanosized cellulose fiber was clearly displayed. In addition, CNF films lacking AgNP-chitosan were also analyzed in this analysis, as shown in Figure 2. (b). The process of producing the CNF film with LiCl/DMAC united several CNFs. Moreover, the morphology of the formed CNF/AgNP-chitosan film is shown in Figure 2 (c). The incorporation of AgNP-chitosan into the CNF matrix via straight film formation was successful. Nanospherical AgNP-chitosan was trapped in the CNF matrix. Further descriptions of the interaction of AgNP-chitosan with the CNF matrix will be elaborated in the functional group analysis.

3.2. Functional group analysis

Samples produced from the straight film formation of CNFs and AgNP-chitosan were analyzed using FTIR spectroscopy to assess the changes in the intensity of functional groups that appeared on CNF/AgNP-chitosan pads compared to pure CNF. Based on the curves shown in Figure 3, some specific peaks representing functional groups in CNF/AgNP-chitosan pads were also found in cellulose macromolecules, i.e., peaks that indicated intramolecular and intermolecular hydrogen bonds at 3332 cm^{-1} and 3298 cm^{-1}, respectively, and the peak confirming O–H bending at 1640 cm^{-1}. Most importantly, peaks at 1428 cm^{-1} and 1165 cm^{-1} were attributed to saccharide molecule and C–O–C bridge stretching, respectively. Meanwhile, C–O stretching was allocated to the peaks at 1053 cm^{-1} and 1030 cm^{-1}. Finally, the β-linkage of cellulose was attributed to the peak at 897 cm^{-1} [9,33].

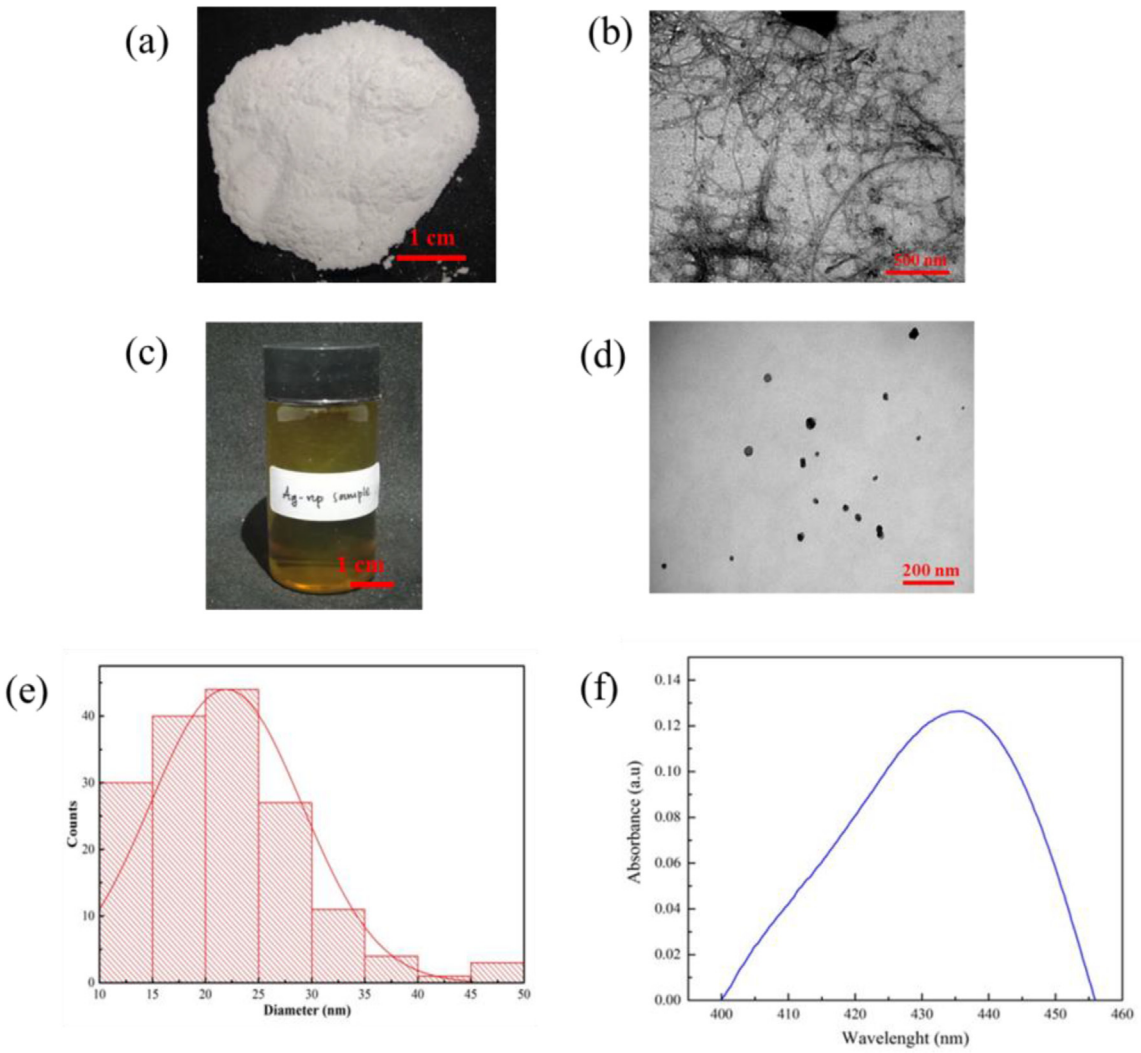

Figure 1. (a) CNF Photograph; (b) TEM image of CNF; (c) AgNP Solution Photograph in Vial Bottle; (d) TEM image of AgNP; (e) Graph of AgNP diameter distribution; and (f) UV-visible spectra of AgNP.

The curves for CNF/AgNP-chitosan pads are shown in Figure 3 (b), (c), (d) and (e). The peak at 881 cm^{-1} in CNF/AgNP-chitosan was larger than that in pure CNF, which suggested the hemiacetal bonding of functional groups between the newly obtained aldehyde groups from chitosan and the hydroxyl groups in cellulose. The C=O bending vibrations in amide I and N– H were assigned to the peak at 3300 cm^{-1}. The O–H and N–H stretching vibrations for CNF/AgNP-chitosan were assigned to peaks at approximately 1653 cm^{-1} and 1599 cm^{-1}, respectively. NH_2 (3358 cm^{-1}) and NH secondary amide vibrations (3288 cm^{-1}) were visible in the stretching vibrations. The peak observed at 1612-1630 cm^{-1} was attributed to carboxylates coordinated with AgNPs [3].

Based on these results, chitosan and AgNPs were chemically bonded and AgNP-chitosan was impregnated in CNFs. Thus, the prepared CNFs had the potential to be used as wound dressings, as the presence of chitosan and AgNPs in CNFs might accelerate the wound healing process.

3.3. XRD analysis

The XRD spectra of the pure CNF and CNF/AgNP-chitosan films are presented in Figure 4. The XRD test performed on the CNF sample showed specific peaks at $2\theta = 14°–18°$, 22.5°, and 34.5°, which corresponded to the (1–10), (110), (200), and (004) cellulose crystal planes, suggesting the formation of cellulose crystal structures [34].

In a past study, the addition of chitosan and AgNPs seemed to affect the crystallinity of CNFs with peak expansions of 25–40°. This expansion might occur because the presence of chitosan and AgNPs in the CNFs damaged the regularity of the CNFs. As a result, CNFs exhibited decreased crystallinity [34]. However, in the present study, the presence of AgNPs did not appear to affect the XRD spectra of the sample. The crystallinity was maintained because the amount of AgNPs on the CNFs was insufficient to alter the XRD pattern [2]. In wound dressing manufacturing, high crystallinity of samples might lead to the formation of microchannel structures, and large surface areas of polymer matrices would potentially affect the drug release properties of the pads [26].

3.4. Thermal analysis

TGA and DTGA curves for pure CNF and CNF/AgNP-chitosan are presented in Figure 5 (a) and (b).

As shown in Figure 5 (a), pure CNFs only experienced a 9% mass loss at temperatures of 70–100 °C. Meanwhile, the largest mass loss (70%) occurred in pads without the addition of AgNP-chitosan at the same temperature. Interestingly, the addition of AgNP-chitosan actually increased the thermal resistance of these pads. This property was observed in CNF/AgNP-chitosan 60:40, which only exhibited 35% weight loss. In this analysis, the derivative TGA (DTGA) curve was also examined to further investigate the thermal properties of the samples

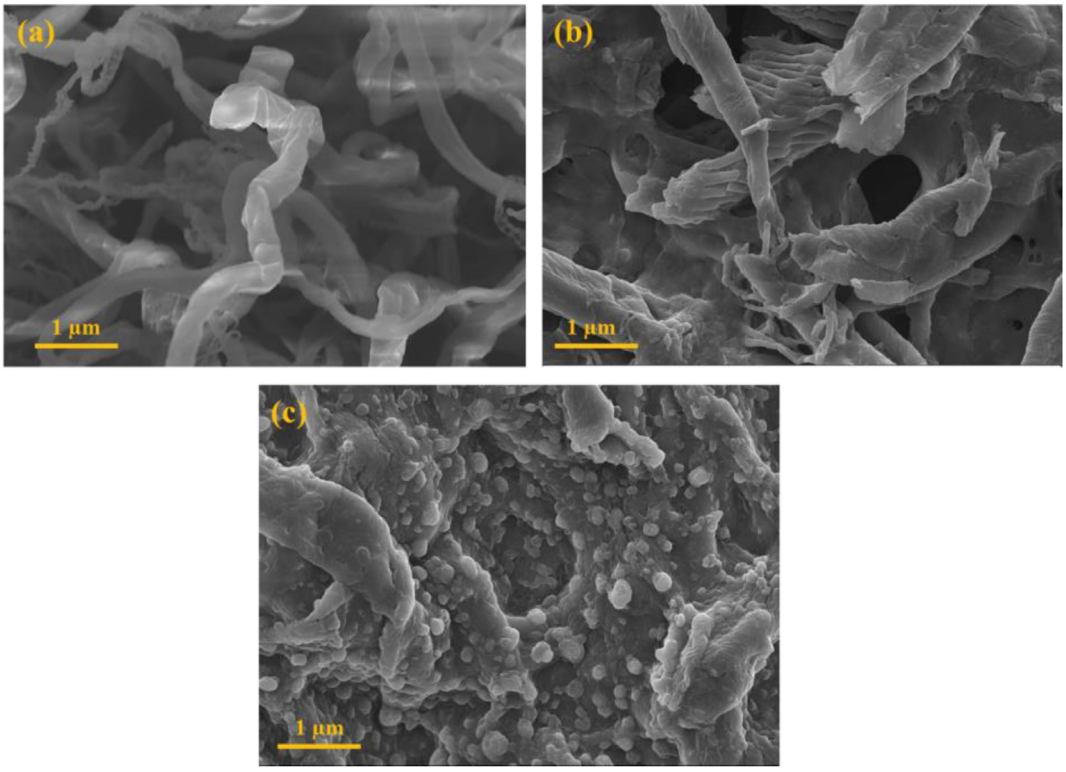

Figure 2. SEM images of (a) Pristine CNF; (b) CNF Film; and (c) CNF/AgNP-chitosan Film.

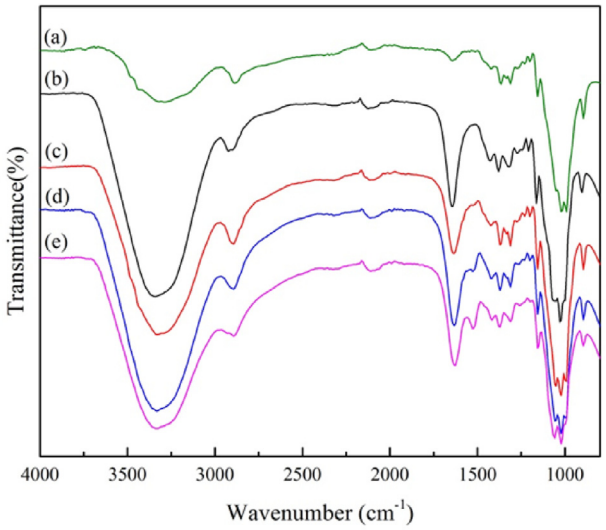

Figure 3. FTIR spectra of (a) pure CNF; (b) CNF/AgNP-chitosan (100:0); (c) CNF/AgNP-chitosan (80:20); (d) CNF/AgNP-chitosan (60:40); and (e) CNF/AgNP-chitosan (50:50).

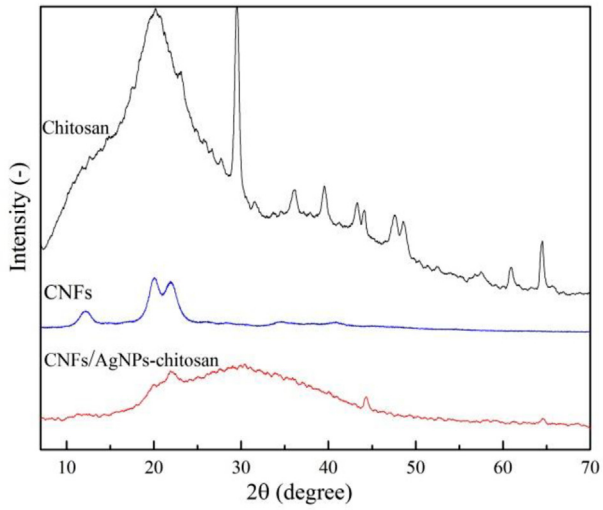

Figure 4. XRD spectra of (a) pure CNF; (b) CNF/AgNP-chitosan (100:0); (c) CNF/AgNP-chitosan (80:20); (d) CNF/AgNP-chitosan (60:40); and (e) CNF/AgNP-chitosan (50:50).

(Figure 5b). The DTGA curve showed only one peak on the CNF curve, while two peaks emerged for the CNF/AgNP-chitosan composite, indicating that maximum mass loss had occurred twice.

As shown in Table 1, the addition of AgNP-chitosan improved the thermal resistance of the pads at the end of the process, where 45%, 28%, 25% and 23% residual masses were detected for CNF/AgNP-chitosan 60:40, CNF/AgNP-chitosan 50:50, CNF/AgNP-chitosan 80:20, and CNF/AgNP-chitosan 100:0, respectively. The higher residual mass of CNF/AgNP-chitosan corresponded to the presence of AgNPs in pads, where Ag experienced thermal degradation at a temperature greater than 600 °C. This result was consistent with previous studies showing that thermal decomposition increased with increasing AgNP loading [35]. The decrease in the thermal resistance of pads was consistent with a number of studies indicating that chitosan has a lower thermal resistance than CNFs [36, 37].

3.5. Antimicrobial properties

Figure 6a shows the antibacterial activity of the CNF/AgNP-chitosan pads compared to the negative control ($P < 0.05$). Among the samples, CNF/AgNP-chitosan 80:20 produced the greatest inhibition zone when incubated with *P. aeruginosa* and *B. subtilis*. The bacterial inhibition power is classified into 4 categories, namely, weak inhibition (<5 mm),

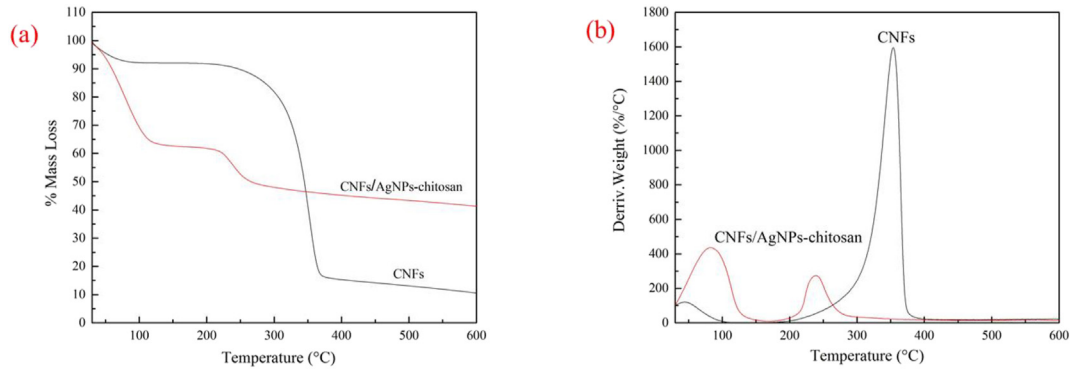

Figure 5. (a) TGA and (b) DTGA curves for CNF and CNF/AgNP-chitosan pad.

Table 1. Samples data of T_5, T_{max} and Residual Mass.

Sample	T_5 (°C)	T_{Max} (°C)		Residual Mass (%)
CNF	53.75	354.8		10.5
Chitosan	47.61	277.2		39.42
CNF/AgNP-chitosan (50:50)	40.07	78.2	213.4	26.56
CNF/AgNP-chitosan (60:40)	46.82	82.4	238.3	42.4
CNF/AgNP-chitosan (80:20)	36.43	74.6	244.4	21.9
CNF/AgNP-chitosan (100:0)	51.49	93.6	233.6	20.74

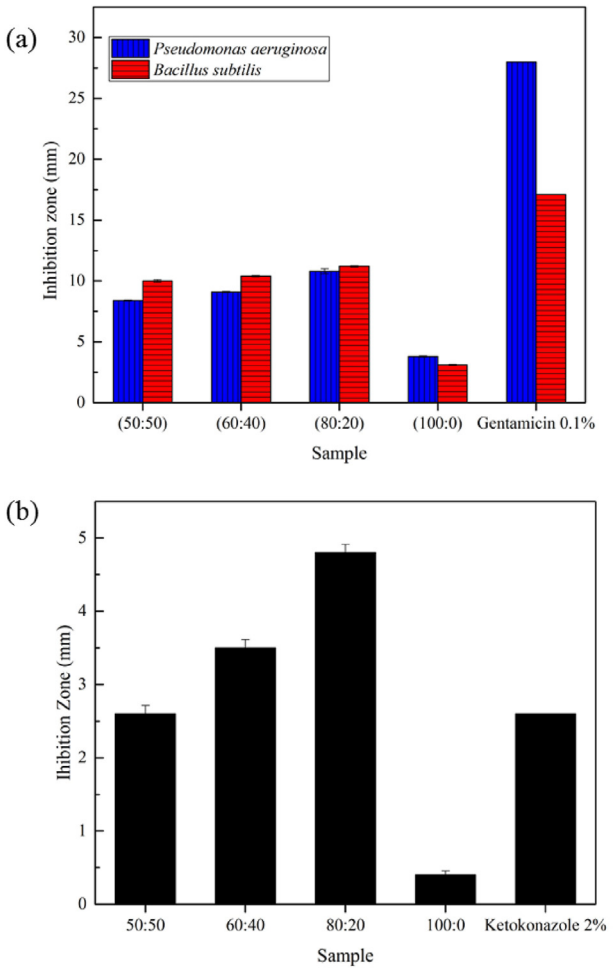

Figure 6. (a) Antibacterial activity against *Pseudomonas aeruginosa* and *Bacillus subtilis*, and (b) Antifugal activity on against *Candida albican* of CNF/AgNP-chitosan pads.

Table 2. Hemocompatibility percentage of CNF/AgNP-chitosan in all variations (n = 5).

Sample	Hemocompatibility (%)
CNF/AgNP-chitosan (50:50)	1.68 ± 0.02
CNF/AgNP-chitosan (60:40)	1.64 ± 0.02
CNF/AgNP-chitosan (80:20)	1.51 ± 0.03
CNF/AgNP-chitosan (100:0)	1.47 ± 0.02

moderate inhibition (5–10 mm), strong inhibition (10–20 mm), and very strong inhibition (>20 mm) [38]. Thus, the CNF/AgNP-chitosan pads had strong bacterial inhibitory activity. This result is consistent with a previous study showing that the inhibitory effect of silver nanoparticles on *B. subtilis* was stronger than on *P. aeruginosa*. A potential explanation for this finding is that the gram-negative bacteria *P. aeruginosa* have an effective permeability barrier, namely, a thin layer of lipopolysaccharide on the outer membrane that limits the penetration of the silver nanoparticle solution. Meanwhile, the gram-positive bacteria *S. aureus* and *B. subtilis* only have a peptidoglycan layer that is more accessible for permeation by silver nanoparticles; therefore, the nanoparticles easily penetrate and damage the bacterial cell walls [37].

Consistent with the antibacterial activity results, the CNF/AgNP-chitosan matrix with a ratio of 80:20 had the greatest inhibition zone when incubated with *Candida albicans* (Figure 6b). This result was supported by previous studies showing that chitosan and AgNPs have strong antimicrobial properties [39, 40]. The results emphasized the use of CNF/AgNP-chitosan films as wound dressings, since the films prevent the growth of *P. aeruginosa* bacteria, which are commonly present in wounds.

3.6. Hemocompatibility

We determined the potential of the materials to be applied as a wound dressing by performing a specific hemocompatibility test. The hemocompatibility test performed on samples referred to ASTM F756-00. All pads showed a hemocompatibility percentage less than 2% (Table 2). Thus, all pads are suitable for further testing in potential applications as wound dressings because the pads produced in the present study meet the requirements for classification as nonhemolytic materials.

4. Conclusions

CNF/AgNP-chitosan films were successfully prepared using straight film formation with different concentration ratios of CNF/AgNP-chitosan, i.e., 100:0, 80:20, 60:40, and 50:50 v/v. CNFs were extracted from OPEFB using the pulping method, followed by acid hydrolysis in 10% HCl. The diameter of the CNFs was approximately 50 nm, while the fiber length was measured in micrometers. The chemical structures of the films, which was characterized by FTIR spectroscopy, showed hemiacetal bonding between CNFs and AgNP-chitosan. The XRD analysis confirmed

that the presence of AgNPs did not alter the crystallinity of the CNFs. The largest thermal degradation was observed when the amount of AgNP-chitosan added was up to 40%. The best antibacterial properties were obtained for CNF/AgNP-chitosan 80:20. All CNF/AgNP-chitosan samples also met the criteria to be classified as nonhemolytic materials. Based on the results of this study, we concluded that CNF/AgNP-chitosan films have great potential as wound dressings. However, further studies, such as in vitro and in vivo tests, are required to elucidate the wound healing properties of CNF/AgNP-chitosan pads.

Declarations

Author contribution statement

Poppy Anjelisa Zaitun Hasibuan: Conceived and designed the experiments; Wrote the paper.

Yuandani; Masitta Tanjung; Saharman Gea: Conceived and designed the experiments; Contributed reagents, materials, analysis tools or data; Wrote the paper.

Khatarina Meldawati Pasaribu; Mahyuni Harahap: Conceived and designed the experiments; Analyzed and interpreted the data; Contributed reagents, materials, analysis tools or data; Wrote the paper.

Yurika Almanda Perangin-Angin; Andre Prayoga; Junius Gian Ginting: Performed the experiments.

Funding statement

This work was supported by Ministry of Research, Technology and Higher Education, Indonesia, through research grant from DRPM 2019 PDUPT number 4537.1/UN5.1.R/PPM/2020.

Data availability statement

Data will be made available on request.

Declaration of interests statement

The authors declare no conflict of interest.

Additional information

No additional information is available for this paper.

Acknowledgements

The authors would like to thank the rector of Universitas Sumatera Utara.

References

[1] P.D. Krishnan, D. Banas, R.D. Durai, D. Kabanov, B. Hosnedlova, M. Kepinska, C. Fernandez, B. Ruttkay-Nedecky, H.V. Nguyen, A. Farid, J. Sochor, V.H.B. Narayanan, R. Kizek, Silver nanomaterials for wound dressing applications, Pharmaceutics 12 (2020) 1–27.

[2] J.U. Shin, J. Gwon, S.Y. Lee, H.S. Yoo, Silver-incorporated nanocellulose fibers for antibacterial hydrogels, ACS Omega 3 (2018) 16150–16157.

[3] M.S. Wang, F. Jiang, Y. Lo Hsieh, N. Nitin, Cellulose nanofibrils improve dispersibility and stability of silver nanoparticles and induce production of bacterial extracellular polysaccharides, J. Mater. Chem. B. 2 (2014) 6226–6235.

[4] S. Gea, K.M. Pasaribu, K. Sebayang, E. Julianti, S.A. Amaturahim, S.U. Rahayu, Y.A. Hutapea, Enhancing the quality of nata de coco starter by channeling the oxygen into the bioreactor through agitation method, 2018, p. 2049, 020064.

[5] M. Rahimi, E.B. Noruzi, E. Sheykhsaran, B. Ebadi, Z. Kariminezhad, M. Molaparast, M.G. Mehrabani, B. Mehramouz, M. Yousefi, R. Ahmadi, B. Yousefi, K. Ganbarov, F.S. Kamounah, V. Shafiei-Irannejad, H.S. Kafil, Carbohydrate polymer-based silver nanocomposites: recent progress in the antimicrobial wound dressings, Carbohydr. Polym. 231 (2020) 115696.

[6] E.A. Kamoun, E.R.S. Kenawy, X. Chen, A review on polymeric hydrogel membranes for wound dressing applications: PVA-based hydrogel dressings, J. Adv. Res. 8 (2017) 217–233.

[7] P. Kaur, V.S. Gondil, S. Chhibber, A novel wound dressing consisting of PVA-SA hybrid hydrogel membrane for topical delivery of bacteriophages and antibiotics, Int. J. Pharm. 572 (2019) 118779.

[8] F. Wang, S. Hu, Q. Jia, L. Zhang, Advances in electrospinning of natural biomaterials for wound dressing, J. Nanomater. 2020 (2020).

[9] K.M. Pasaribu, S. Gea, S. Ilyas, T. Tamrin, A.A. Sarumaha, A. Sembiring, I. Radecka, Fabrication and In-Vivo Study of Micro-colloidal Zanthoxylum Acanthopodium-Loaded Bacterial Cellulose as a Burn Wound Dressing, Polymers (Basel). (n.d.).

[10] N. Ahmad, M.M. Ahmad, N.K. Alruwaili, Z.A. Alrowaili, F.A. Alomar, S. Akhtar, O.A. Alsaidan, N.A. Alhakamy, A. Zafar, M. Elmowafy, M.H. Elkomy, Antibiotic-Loaded Psyllium Husk Hemicellulose and Gelatin-Based Polymeric Films for Wound Dressing Application, 2021, pp. 1–15.

[11] A. Akhmetova, A. Heinz, Electrospinning proteins for wound healing purposes: opportunities and challenges, Pharmaceutics 13 (2021) 1–22.

[12] I.K. Siakavella, F. Lamari, D. Papoulis, M. Orkoula, P. Gkolfi, M. Lykouras, K. Avgoustakis, S. Hatziantoniou, Effect of plant extracts on the characteristics of silver nanoparticles for topical application, Pharmaceutics 12 (2020) 1–17.

[13] Z. Edis, S.H. Bloukh, M.R. Ibrahim, H.A. Sara, "Smart" antimicrobial nanocomplexes with potential to decrease surgical site infections (SSI), Pharmaceutics 12 (2020) 1–36.

[14] H. Bardania, R. Mahmoudi, H. Bagheri, Z. Salehpour, M.H. Fouani, B. Darabian, S.S. Khoramrooz, A. Mousavizadeh, M. Kowsari, S.E. Moosavifard, G. Christiansen, D. Javeshghani, M. Alipour, M. Akrami, Facile preparation of a novel biogenic silver-loaded Nanofilm with intrinsic anti-bacterial and oxidant scavenging activities for wound healing, Sci. Rep. 10 (2020) 1–14.

[15] J. Azeredo, N.F. Azevedo, R. Briandet, N. Cerca, T. Coenye, A.R. Costa, M. Desvaux, G. Di Bonaventura, M. Hébraud, Z. Jaglic, M. Kačániová, S. Knøchel, A. Lourenço, F. Mergulhão, R.L. Meyer, G. Nychas, M. Simões, O. Tresse, C. Sternberg, Critical review on biofilm methods, Crit. Rev. Microbiol. 43 (2017) 313–351.

[16] J. Wu, Y. Zheng, W. Song, J. Luan, X. Wen, Z. Wu, X. Chen, Q. Wang, S. Guo, In situ synthesis of silver-nanoparticles/bacterial cellulose composites for slow-released antimicrobial wound dressing, Carbohydr. Polym. 102 (2014) 762–771.

[17] J. Tian, K.K.Y. Wong, C.M. Ho, C.N. Lok, W.Y. Yu, C.M. Che, J.F. Chiu, P.K.H. Tam, Topical delivery of silver nanoparticles promotes wound healing, ChemMedChem 2 (2007) 129–136.

[18] N. Duraipandy, R. Lakra, K. Vinjimur Srivatsan, U. Ramamoorthy, P.S. Korrapati, M.S. Kiran, Plumbagin caged silver nanoparticle stabilized collagen scaffold for wound dressing, J. Mater. Chem. B. 3 (2015) 1415–1425.

[19] A.A. Jack, H.R. Nordli, L.C. Powell, K.A. Powell, H. Kishnani, P.O. Johnsen, B. Pukstad, D.W. Thomas, G. Chinga-Carrasco, K.E. Hill, The interaction of wood nanocellulose dressings and the wound pathogen P. aeruginosa, Carbohydr. Polym. 157 (2017) 1955–1962.

[20] J. Moohan, S.A. Stewart, E. Espinosa, A. Rosal, A. Rodríguez, E. Larrañeta, R.F. Donnelly, J. Domínguez-Robles, Cellulose nanofibers and other biopolymers for biomedical applications. A review, Appl. Sci. 10 (2020).

[21] E. Espinosa, D. Filgueira, A. Rodríguez, G. Chinga-Carrasco, Nanocellulose-based inks—effect of alginate content on the water absorption of 3D printed constructs, Bioengineering 6 (2019).

[22] C.T. Handoko, A. Huda, M.D. Bustan, B. Yudono, F. Gulo, Green synthesis of silver nanoparticles and its antibacterial activity: a review, Rasayan J. Chem. 10 (2017) 1137–1144.

[23] C.T. Handoko, N.G. Moustakas, T. Peppel, A. Springer, F.E. Oropeza, A. Huda, M.D. Bustan, B. Yudono, F. Gulo, J. Strunk, Characterization and effect of Ag(0) vs. Ag(I) species and their localized plasmon resonance on photochemically inactive TiO 2, Catalysts 9 (2019).

[24] X.F. Zhang, Z.G. Liu, W. Shen, S. Gurunathan, Silver nanoparticles: synthesis, characterization, properties, applications, and therapeutic approaches, Int. J. Mol. Sci. 17 (2016).

[25] M. Bin Ahmad, J.J. Lim, K. Shameli, N.A. Ibrahim, M.Y. Tay, Synthesis of silver nanoparticles in chitosan, gelatin and chitosan/gelatin bionanocomposites by a chemical reducing agent and their characterization, Molecules 16 (2011) 7237–7248.

[26] K.M. Pasaribu, S. Gea, S. Ilyas, T. Tamrin, I. Radecka, Characterization of bacterial cellulose-based wound dressing in different order impregnation of chitosan and collagen, Biomolecules 10 (2020) 1–15.

[27] S. Gea, A.H. Siregar, E. Zaidar, M. Harahap, D.P. Indrawan, Y.A. Perangin-Angin, Isolation and characterisation of cellulose nanofibre and lignin from oil palm empty fruit bunches, Materials 13 (2020) 2290.

[28] E. Marusich, Fatty acids from *Hermetia illucens* larvae fat inhibit the proliferation and growth of actual phytopathogens, Microorganisms (2020).

[29] D.A. Mosselhy, Silica–gentamicin nanohybrids: combating antibiotic resistance, bacterial biofilms, and in vivo toxicity, Int. J. Nanomed. (2018).

[30] J.H. Jorgensen, M.J. Ferraro, Antimicrobial susceptibility testing: a review of general principles and contemporary practices, Clin. Infect. Dis. 49 (2009) 1749–1755.

[31] F.D. Montana, Effectiveness of cocoa (*Theobroma cacao* L.) Seed extract on the growth of in vitro malassezia furfu, International conference of public health (2020).

[32] E. Misran, B. Wirdjosentono, N.M. Noor, S. Gea, S.A. Situmorang, M. Harahap, Preparation and Characterisation of Electrospun Composite Nanofibre Polyvinyl Alcohol/Nanofibrillated Cellulose Isolated from Oil Palm Empty Fruit Bunches, BioResources, 2020.

[33] Z. Yu, W. Wang, F. Kong, M. Lin, A. Mustapha, Cellulose nanofibril/silver nanoparticle composite as an active food packaging system and its toxicity to human colon cells, Int. J. Biol. Macromol. 129 (2019) 887–894.

[34] Q. Xu, Y. Ji, Q. Sun, Y. Fu, Y. Xu, L. Jin, Fabrication of cellulose nanocrystal/chitosan hydrogel for controlled drug release, Nanomaterials 9 (2019).

[35] H. Ito, M. Sakata, C. Hongo, T. Matsumoto, T. Nishino, Cellulose nanofiber nanocomposites with aligned silver nanoparticles, Nanocomposites 4 (2018) 167–177.
[36] Y. Wang, K. Uetani, S. Liu, X. Zhang, Y. Wang, P. Lu, T. Wei, Z. Fan, J. Shen, H. Yu, S. Li, Q. Zhang, Q. Li, J. Fan, N. Yang, Q. Wang, Y. Liu, J. Cao, J. Li, W. Chen, Multifunctional bionanocomposite foams with a chitosan matrix reinforced by nanofibrillated cellulose, ChemNanoMat 3 (2017) 98–108.
[37] S.C.M. Fernandes, C.S.R. Freire, A.J.D. Silvestre, C. Pascoal Neto, A. Gandini, L.A. Berglund, L. Salmén, Transparent chitosan films reinforced with a high content of nanofibrillated cellulose, Carbohydr. Polym. 81 (2010) 394–401.
[38] W.W. Davis, T.R. Stout, Disc plate method of microbiological antibiotic assay. I. Factors influencing variability and error, Appl. Microbiol. 22 (1971) 659–665.
[39] P. Sahariah, M. Másson, Antimicrobial chitosan and chitosan derivatives: a review of the structure-activity relationship, Biomacromolecules 18 (2017) 3846–3868.
[40] G. Franci, A. Falanga, S. Galdiero, L. Palomba, M. Rai, G. Morelli, M. Galdiero, Silver nanoparticles as potential antibacterial agents, Molecules 20 (2015) 8856–8874.